Journal of Environmental Health Science and Engineering (2022) 20:849–860
https://doi.org/10.1007/s40201-022-00825-y

RESEARCH ARTICLE

High efficiency of magnetite nanoparticles for the arsenic removal from an aqueous solution and natural water taken from Tambo River in Peru

M. Huanca Ccamerccoa[1] · N. L. Tapia Falcon[1] · L. León Félix[2] · D. G. Pacheco-Salazar[2] · F. F. H. Aragón[2,3] · J. A. H. Coaquira[2,3] · Jéremie Garnier[4] · C. Vera-Gonzales[1]

Received: 30 January 2021 / Accepted: 9 August 2022 / Published online: 14 September 2022
© The Author(s), under exclusive licence to Tehran University of Medical Sciences 2022

Abstract

Water is an essential compound on earth and necessary for life. The presence of highly toxic contaminants such as arsenic and others, in many cases, represents one of the biggest problems facing the earth´s population. Treatment of contaminated water with magnetite (Fe_3O_4) nanoparticles (NPs) can play a crucial role in arsenic removal. In this report, we demonstrate arsenic removal from an aqueous solution and natural water taken from the Peruvian river (Tambo River in Arequipa, Peru) using magnetite NPs synthesized by the coprecipitation method. XRD data analysis of Fe_3O_4 NPs revealed the formation of the cubic-spinel phase of magnetite with an average crystallite size of ~13 nm, which is found in good agreement with the physical size assessed from TEM image analysis. Magnetic results evidence that our NPs show a superparamagnetic-like behavior with a thermal relaxation of magnetic moments mediated by strong particle-particle interactions. FTIR absorption band shows the interactions between arsenate anions and Fe-O and Fe-OH groups through a complex mechanism. The experimental results showed that arsenic adsorption is fast during the first 10 min; while the equilibrium is reached within 60 min, providing an arsenic removal efficiency of ~97%. Adsorption kinetics is well modeled using the pseudo-second-order kinetic equation, suggesting that the adsorption process is related to the chemisorption model. According to Langmuir's model, the maximum arsenic adsorption capacity of 81.04 $mg \cdot g^{-1}$ at pH = 2.5 was estimated, which describes the adsorption process as being monolayer, However, our results suggest that multilayer adsorption can be produced after monolayer saturation in agreement with the Freundlich model. This finding was corroborated by the Sips model, which showed a good correlation to the experimental data. Tests using natural water taken from Tambo River indicate a significant reduction of arsenic concentration from 356 μg L^{-1} to 7.38 μg L^{-1}, the latter is below the limit imposed by World Health Organization (10 μg L^{-1}), suggesting that magnetite NPs show great potential for the arsenic removal.

Keywords Arsenic · Magnetite · Nanoparticles · Removal

✉ F. F. H. Aragón
ffharagon@gmail.com

1 Departamento de Química, Universidad Nacional de San Agustín de Arequipa. Laboratorio LAPCI-Nano, Independencia s/n, Arequipa, Perú

2 Laboratorio de Películas Delgadas, Universidad Nacional de San Agustín de Arequipa, Escuela Profesional de Física, Av. Independencia s/n, Arequipa, Perú

3 Instituto de Física, Núcleo de Física Aplicada, Universidade de Brasília, 70910-900 Brasília, DF, Brazil

4 Instituto de Geociências, Universidade de Brasília, Campus Darcy Ribeiro, L2, Asa Norte, 70910900 Brasília, Distrito Federal, Brazil

Introduction

Arsenic is one of the contaminants that are present on earth and can seep into groundwater. Also, arsenic is present in the air of urban and industrial plants. Nonetheless, where arsenic contamination does occur, it represents a significant risk to human beings' health worldwide. Besides, the main concerns related to arsenic are long-term exposure that may cause cancer (also severe skin lesions, dermatitis, respiratory, urinary tract, kidneys, liver, and lungs diseases [1, 2]) and the incidence in the frequency of other diseases [3, 4]. Due to the human health risk as a potential carcinogenic

effect, the World Health Organization (WHO) has established a maximum arsenic concentration of less than 10 µg L^{-1}[5] in drinking water to minimize the risk to human being's health. Numerous countries have then adopted this new limit all over the world, such as Peru, where the Ministry of Health's ordinance, which regulates the quality of drinking water, also indicates a maximum value permitted of 10 µg L^{-1} of arsenic by the Water Quality Regulations for Human Consumption (D.S. N° 031-2010-S. A, 2010). Given the high risk of arsenic exposure, there is a growing interest in using cost-effective materials and methods to extract them from water and provide less polluted water, which is a study issue currently [6]. In this context, the adsorption method has been recognized as a promising technique for removing arsenic from water samples due to being the simplest, most cost-effective, and user-friendly [7]. Adsorption efficiency strongly depends on the type of adsorbents. In this regard, several materials were used for water remediation, which we can highlight the use of *Moringa peregrina* seed [8], graphite oxide [9], iron oxides 10–12, among others. Nanomaterials based adsorbents such as iron oxide nanoparticles are outstanding adsorbents for arsenic removal because of the strong interaction between arsenic and iron oxide (Fe-O-As) that are highly attractive merits of magnetic adsorbents [13]. Magnetite (Fe_3O_4) NPs are an iron-oxide mineral that can be synthesized through coprecipitation, hydrothermal, thermal decomposition, and sol-gel methods. The main benefit of the optimized and scalable synthesis coprecipitation method is that the effect of temperature, pH, and agitation velocity are important variables that give the magnetite NPs specific size important characteristics [14]. In addition, many researchers have reported that the adsorption capacity of magnetite NPs from 1.30 to 66.53 mg g^{-1}10, 11 for total arsenic removal, from 1.33 to 68.3 mg $g^{-1}$for arsenic (III) [15, 16]· and from 0.35 to 85.3 mg $g^{-1}$for arsenic(V)16–19 by the kinetics model. Hence, some of the strategies to improve the adsorption capacity of arsenic depend on the adsorbent size [20, 21], the increase in the adsorption surface area and active sites of the adsorbents [22], and the co-existing cations in aqueous solution do not show any significant effect on As (V) removal efficiency [17]. Iron and its compounds are known as the most effective adsorbents but strongly depend on the pH of the solution [17].

This study aims to prove the excellent efficiency of magnetite nanoparticles for arsenic removal from contaminated water samples, using a single one-step chemical route to prepare the nanoparticles. The adsorption capacity of Fe_3O_4NPs was tested by varying parameters such as adsorbent dose, pH of the solution, and contact time. Finally, our experimental data were fitted with the kinetic and isothermal models, Fe_3O_4 NPs are being used for water remediation of the Tambo river in Peru, which is known to have a larger percentage of arsenic than is allowed for human consumption.

Materials and methods

The Fe_3O_4 nanoparticles were synthesized by the chemical coprecipitation method, where the Fe(II) sulphate and Fe(III) chloride in a relation of 2:1 were dissolved in 100 mL of ultrapure water. The mixed solution was heated up to80 ºCunder constant agitation. Subsequently, a NaOH (5 M) reducing solution was added until reaching pH10 and was left in agitation for 30 min. All process was kept in an inert nitrogen atmosphere. Then, the synthesized nanoparticles were washed several times with absolute ethanol until obtaining a pH similar to 7. Finally, the nanoparticles were taken to an oven at 40 °C for 24 h. The samples were characterized by X-ray diffraction (XRD) and Fourier transform infrared spectroscopy (FTIR) measurements, concerning the XRD patterns were obtained via Rigaku Miniflex 600 diffractometer using Cu-Kα radiation (0.15418 nm). Transmission Electron Microscopy (TEM) images were obtained using a Jeol JEM-1011 microscope. Superconducting Quantum Interference Device- SQUID (Quantum Design, model MPMS3) was used to obtain the *M* vs. *H* and *M* vs. *T* curves, the latter with applied magnetic fields up to 50 Oe and temperature in the range of 5 – 340 K. Mössbauer measurements were carried out in the conventional transmission geometry using a 57Co/Rh source. The FTIR measurements were performed by a mode ATR-FTIR spectrometer (Bruker, model Tensor 27). Arsenic concentration in aqueous solutions was measured by inductively coupled plasma - optical emission spectrometry (ICP-OES) (Agilent technologies, model 5100). To study the arsenic remotion, the arsenic stock solution was prepared by dissolving arsenic acid (H_3AsO_4) (Merck Millipore) in ultrapure water. The effect of the pH on the removal of arsenic was studied by working solution, which is adjusted using HCl and NaOH solution standards. A solution of arsenic (V) at a concentration of 0.31 mg L^{-1} was prepared from arsenic acid (H_3AsO_4) at 1000 mg L^{-1}at pH 2.5, and 5 mg of absorbent (Fe_3O_4 NPs) was added. It was sonicated for 8 h, taking out aliquots in 5, 10, 15, 30, 240, and 480 min. The samples extracted each time were filtered using a 0.2 µm microfilter to be analyzed by the ICP-OES technique. For the triple measurement, the lowest analyte concentration (LOQ) was 0.0055 ppm, while the technique's limit of detection (LOD) is 0.0017. Water samples were taken from the Tambo River, which is located in Islay province within the department of Arequipa-Peru (see Fig. 1). The name only refers to a relatively short section; about 159 km long. It starts at the confluence of the Ene and Perené Rivers in the town of Puerto Prado. This

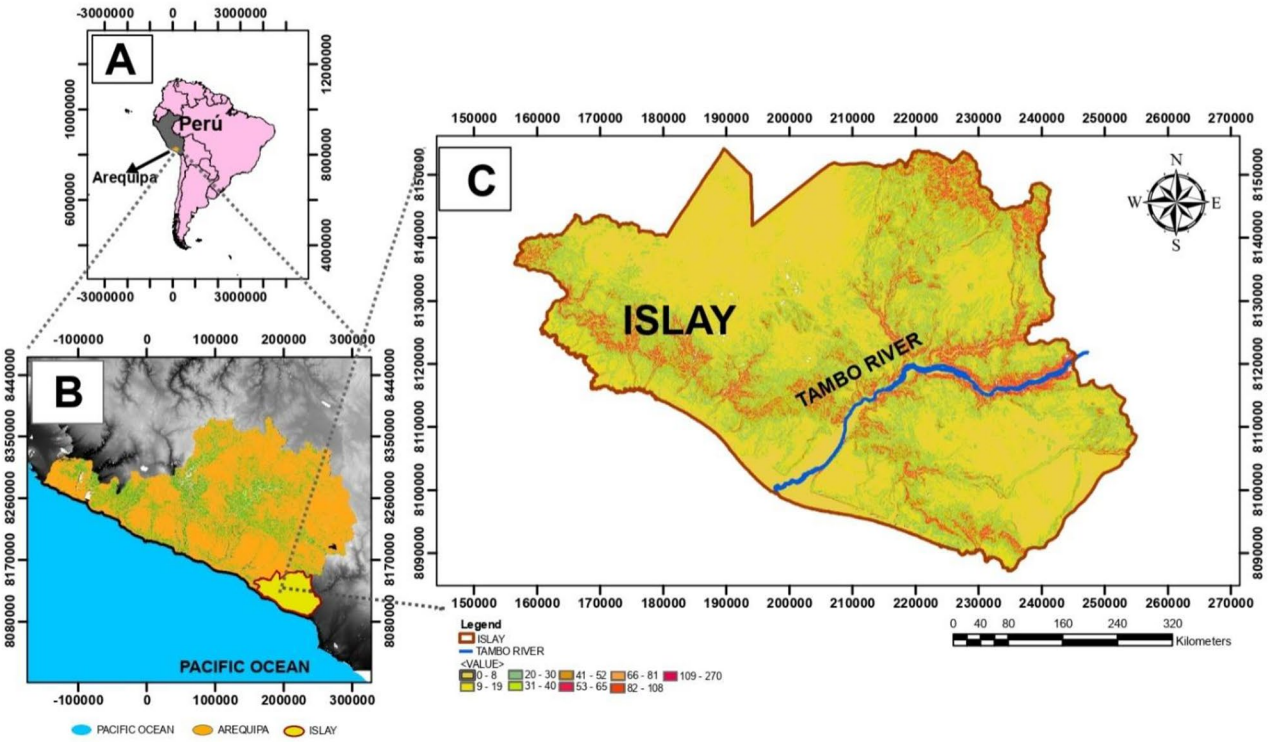

Fig. 1 Location map of the Tambo River from the water sample is collected. (A) South America; (B) State of Arequipa in Peru; (C) Islay province within the state of Arequipa

river's water is known for the use of irrigation and the use of the people. To determine the initial concentration of the sample, it was firstly analyzed, and has been found an initial arsenic concentration of 267.1 μg L^{-1} was measured by the ICP-OES technique, this value is higher than the permitted by the local agency of water control. It's worth noting that the arsenic removal experiment was carried out in triplicate, with the average value used in the analyses.

Finally, for the isotherm study, experiments were carried out with 141, 310, and 531 μgL^{-1} initial concentration of arsenic(V) at pH 2.5. The arsenic solutions were added to 5 mg L^{-1} magnetite NPs.The mixture was kept on constant stirring for 8 h. After, the samples were analyzed by ICP-OES.

Results and discussion

Figure 2 shows the structural characterization by the X-ray diffraction data analysis of the Fe_3O_4 NPs after the As (V) adsorption onto the magnetite surface (As-Fe_3O_4). The diffraction pattern was refined using the Rietveld refinement method, which indicates that all diffraction peaks correspond to the cubic spinel phase of magnetite (space group: Fd-3 m). A similar pattern was obtained for the Fe_3O_4 NPs before the As (V) adsorption (data not shown here). The obtained lattice parameter was ≈ 8.327 Å, which is in agreement with values reported for the corresponding bulk magnetite [23]. However, the As phase has not been observed, suggesting that As (V) was adsorbed onto the NPs surface to maintain the crystal structure of magnetite [24]. To assess the crystallite size, the Scherrer`s equation and the linewidth at half maximum of all diffraction peaks were used. Our results display the same crystallite size of ~ 13 nm for the Fe_3O_4 NPs after and before the As (V) adsorption, suggesting that there are no changes in the crystal structure. In addition, TEM image was used to confirm the crystallite size determined from XRD study. Figure 2 (b) shows the transmission image of nanoparticles, an average physical crystallite size of 13.5 ± 0.2 nm obtained after a frequency count of around N = 200 particles and was fitting using a LogNormal function (continuing red line, in the inset Fig. 2 (b)), being in a good agreement with results of XRD.

Figure 3(a) displays the magnetization curves as a function of the applied magnetic field performed for the Fe_3O_4 NPs at 300 K and 5 K. As observed, the M vs. H curve at 300 K is consistent with relaxed states, meanwhile, at 5 K the irreversible features, indicate blocked states, evidencing a strong temperature-dependent behavior such as superparamagnetism. A remanence magnetization of M_R ~23.2 emu/g

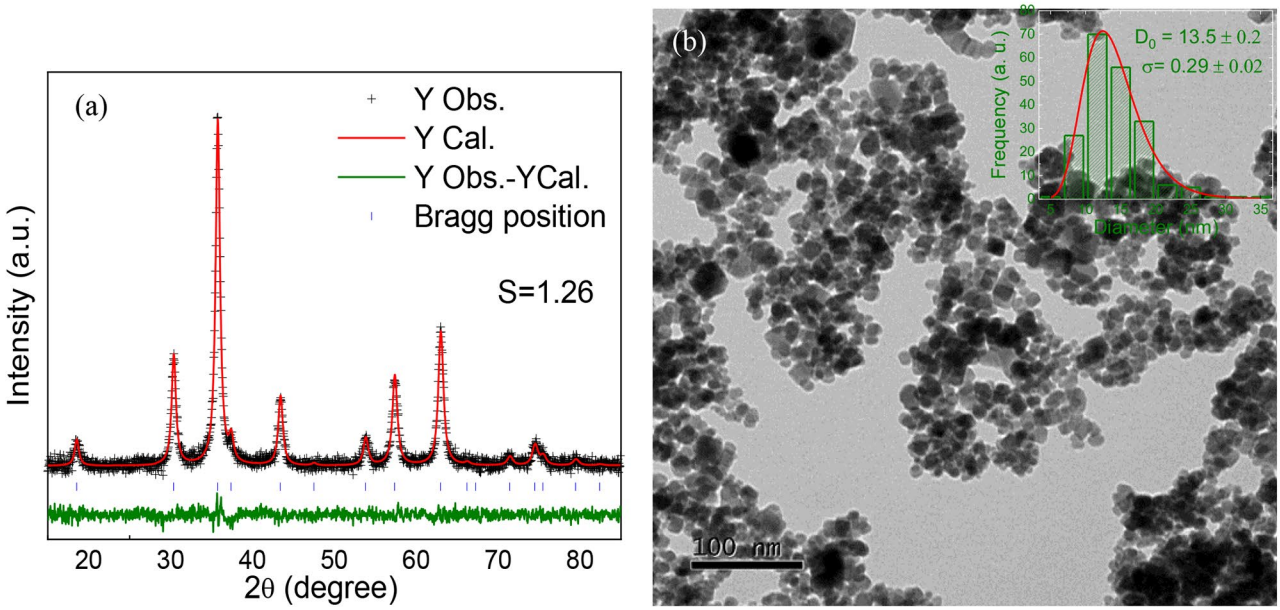

Fig. 2 (a) Room temperature XRD pattern of Fe_3O_4 NPs. The points represent the experimental data, the solid red line is the calculated curve from the Rietveld analysis, and the green line at the bottom is the difference between them, the blue lines are the expected positions corresponding to the Bragg planes to the magnetite structure. S is a parameter that quantifies the quality of the refinement. (b) TEM micrograph and its corresponding histogram used to determine the average physical size and polydisperse index

and a coercive field of H_C~ 343 Oe are determined from the *M* vs. *H* curve at 5 K. The ratio *Mr/Ms* obtained at 5 K was 0.26 for our sample, indicating the occurrence of interacting particles [25]. Besides, we use the law of approach to saturation: $M = M_S\left(1 - b/H^2\right)$, where M_S is a saturation magnetization, and *b* is a constant correlated with the magnetic anisotropy constant to obtain more information. From the data fit in the high field region (see Fig. 3 (a)) a M_S ~91 and ~83 emu/g were determined for *M* vs. *H* curves at 5 and 300 K, respectively. The latter is in agreement with that reported in the literature for bulk Fe_3O_4 [26]. Figure 3 (b) are shown the zero–field-cooled (ZFC) and field-cooled (FC) magnetization curves of the sample. As observed, both curves show irreversibilities below 340 K. The ZFC curve shows an increasing trend with the temperature and no clear maximum, but a broad shoulder at ~200 K is discerned. Contrary to what is expected, due to the particle size, the growing trend of the ZFC curve strongly suggests the occurrence of particle-particle interactions, which likely reflects the formation of aggregates. Mössbauer spectrum obtained at room temperature is consistent with a blocked state even at 300 K (see Fig. 3(c)). The spectrum is well modeled with two sextets and the origin of these sextets is assigned to Fe^{3+} ions occupying both the tetrahedral and octahedral sites due to the hyperfine parameters obtained from the fits: isomer shift, IS ~ 0.22 mm/s (~ 0.25 mm/s)and hyperfine magnetic field of H_{eff} ~ 49 T (45 T) assigned to the tetrahedral (octahedral) sites in the spinel structure.

ATR-FTIR studies were conducted to examine the functional groups present in the magnetite NPs surface before and after arsenic adsorption. As shown in Fig. 4, the transmittance as a function of the wavenumber, the bands between 565 and 700 cm^{-1} were attributed to the Fe-O stretching vibrations in iron oxide 27–29. The FTIR spectrum before and after arsenic adsorption shows bands at ~ 549 cm^{-1}, and ~ 624 cm^{-1} which are related to Fe-O vibration characteristic of the magnetite phase [10], these bands have been not displayed changes after the As (V) adsorption suggesting that the magnetite do not show major structural alterations, in good agreement with the XRD results. However, some differences have been observed after the removal of As(V) such as (i) the decreasing of the bands located at ~ 1635 and ~ 3394 cm^{-1} correlated with the OH vibration of the physically adsorbed water 30, this behavior can be associated to the fact that in an aqueous medium, the Fe and O atoms on the magnetite NPs surface increase the hydroxyl groups (-OH), meanwhile, these groups in the As(V) presence can be form arsenic complexes [31, 32], provoke a reduction of the OH groups, this fact can explain the observed reduction of the vibration modes related to the hydroxyl groups after As (V) adsorption. (ii) The rise up of the bands at ~ 1049 cm^{-1} and ~ 1399 cm^{-1}, located in the fingerprint region, exhibited in the magnetite sample after As (V) adsorption could be associated with arsenic composite on the particle surface.

The pH effect on arsenic removal efficiency is depicted in Fig. 5. The experiments were carried out at room

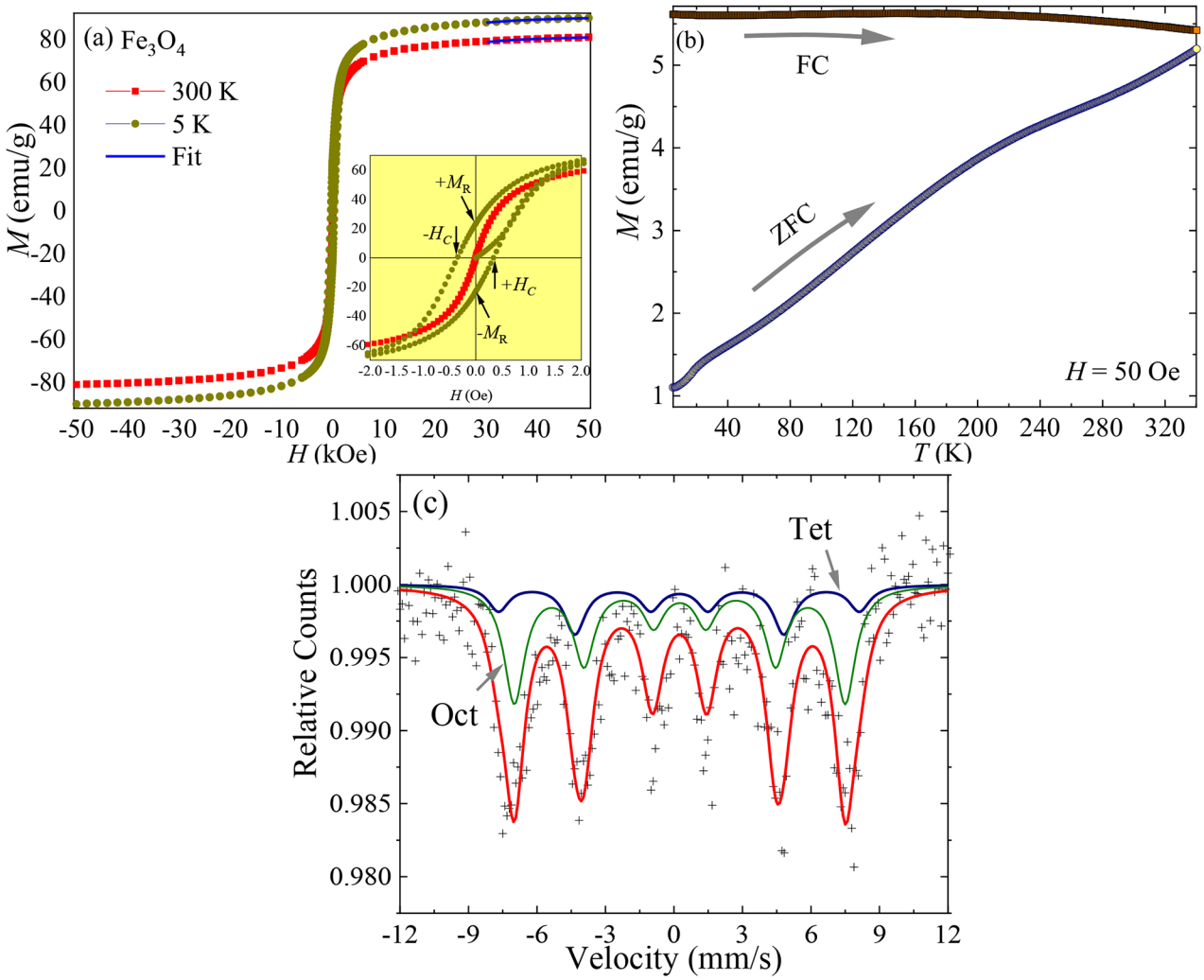

Fig. 3 (a) Magnetization as a function of the applied magnetic field (*H*) curves of the Fe_3O_4 nanoparticles at 300 K and 5 K. The inset shows a magnification of the *M* vs. *H* curve in the low field region. (b) ZFC and FC curves were recorded by applying an external magnetic field of 50 Oe, and (c) Mössbauer spectrum of Fe_3O_4 NPs obtained at room temperature. The cross represents the experimental data and the red line is the calculated one

temperature and conducted at pH 2.5 and 7.5 at different contact times with a fixed nanoparticles concentration of 5000 μg L^{-1} that was put in contact with an initial arsenic solution concentration of355 μg L^{-1}. The results showed that the highest arsenic adsorption onto magnetite was at pH 2.5, and it showed a decrease in pH 7.5. However, the arsenic adsorption in both pH 2.5 and pH 7.5 was not different before 30 min of contact time. After 8 h, the maximum removal percentages of arsenic were 90% and 40% for pH 2.5 and pH 7.5, respectively. It suggested that As(V) adsorption onto Fe_3O_4 NPs surface is more efficient in an acid pH. These results are in good agreement with the literature, for instance, Kango reported that using sand-coated magnetite NPs, the total removal percentage of As(V) was 99.99% at pH 2 17, 33. The arsenic adsorption showed a decrease as the pH increased 18, 34, 35. The variation in As (V) removal efficiency at these pH values may be attributed to different affinities of magnetite NPs for different species of As(V). In aqueous media at low pH, the magnetite NPs surface is coated by positively charged species such as Fe^{2+}, $FeOH^{+}$, iron (III) hydroxide ($Fe(OH)^{3+}$) 36, iron II hydroxides ($Fe(OH)^{2+}$) 37, 39, 40, 43. Since arsenic dissociates in the form of $H2AsO^{4-}$ (negatively charged species) with a pH in the range from 2.2 to 7 [6, 30, 38]; meanwhile, for pH in the range from 6 to 8, the arsenic species are $HAsO^{4-}$ and $HAsO4^{2-}$, and for higher pH (ranging from 7 or 8 to 11) the $HAsO_4^{2-}$ dominants [38–40]. Other authors reported that a pH 4 can already find $HAsO_4^{-2}$[41, 42]. The explanation for this behavior could be related to the distribution of As (V) species in the aqueous medium, when the concentration of arsenic increases, the pH used for adsorption decreases [38].On the other hand, As could also bind to the

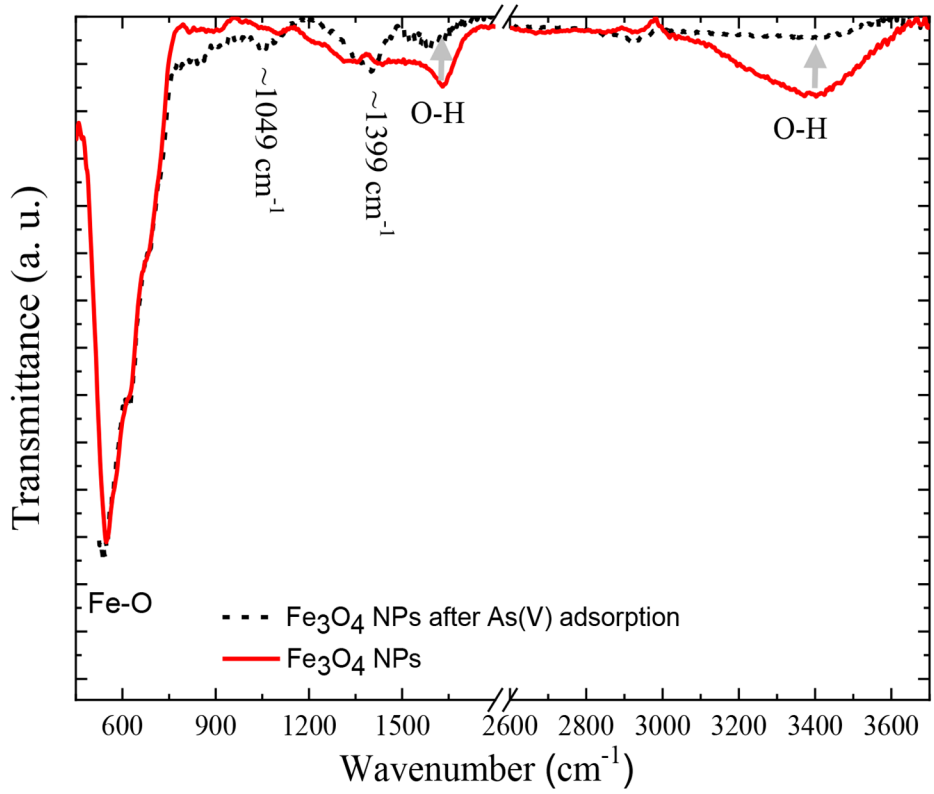

Fig. 4 TIR spectrum of before and after As (V) adsorption onto magnetite. (As solution prepared in the laboratory)

Fe_3O_4 NPs surface by electrostatic interaction [43]. This interaction would be affected by an increase in pH causing a reduction in the As (V) adsorption or competition between hydroxyl ions and arsenic species, for adsorption sites [39], or both As species can be effectively adsorbed by NPs. This explains why the arsenic adsorption onto Fe_3O_4 NPsare better for acidic pH values than for higher pH values [39, 40].

After the optimal determination of the pH value (acid) for As adsorption, the effect of the adsorbent dosage (5000 μg L^{-1} and 10,000 μg L^{-1}) for the arsenic removal from a prepared solution was evaluated at different times (from 10 to 2880 min). The adsorption results obtained for an arsenic concentration of 355 μg L^{-1} and pH 2.5 was rapid in the first 10 min, as shown in Fig. 6. The removal percentage initially increases with the adsorbent dosage increase. An arsenic adsorption percentage of 83.7% and 95.4%, was obtained for 5000 μg L^{-1} and 10,000 μg L^{-1}, respectively. The fast adsorption at the initial stage could be due to probably the increase in adsorbate concentration in the adsorbent as there must be an increased number of available active sites due to the over-crowding of particles. As the contact time elapses, the active sites are saturated with more arsenic ions or slower mass transfer. Arsenic adsorption on Fe_3O_4 NPs is contact time-dependent. After 1 h of contact, stability in the adsorption rate and a removal percentage (with an average value of 95%) were determined for both masses. As adsorbent dosage showed similar adsorption trends, we decide to work with the lower adsorbent dosage (5000 μg L^{-1}) of Fe_3O_4 NPs that are enough to get good removal efficiencies.

The adsorption equilibrium of arsenic on Fe_3O_4 NPs exhibited faster kinetics and after 10 min, the initial arsenic concentration of 310 μgL^{-1} was reduced 28.3 μgL^{-1}. Longer contact periods (60 min) were required to reach the adsorption equilibrium of 3.25 μgL^{-1}, which is below the limit value (10 μgL^{-1}) imposed by WHO in water [5]. The arsenic removal efficiency was 90% and 99% at 10 and 60 min, respectively. The rapid adsorption rate and high arsenic removal efficiency could be related to the high surface area, pore volume, and the formation of complexes or electrostatic interactions [44]. In order to understand the adsorption mechanism and the efficiency of the NPs, the experimental data were analyzed with kinetic models as the pseudo-first-order (Eq. (1)) and the pseudo-second-order (Eq. (2)) kinetic models [45, 46] (see Fig. 7)that are expressed as:

$$\mathrm{Ln}\,(q_e - q_t) = \mathrm{Ln}q_e - k_1 t \tag{1}$$

$$\frac{t}{q_t} = \frac{1}{k_2 q_e^2} + \frac{t}{q_e} \tag{2}$$

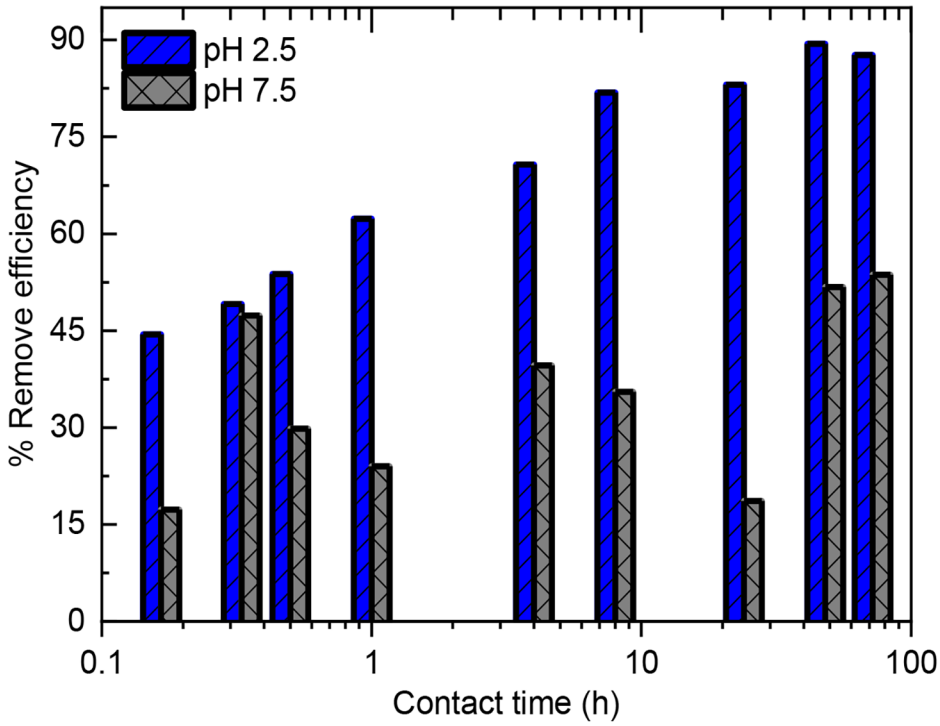

Fig. 5 Effect of pH in the percentage of As (V) adsorption onto magnetite NPs surfaces at different contact time

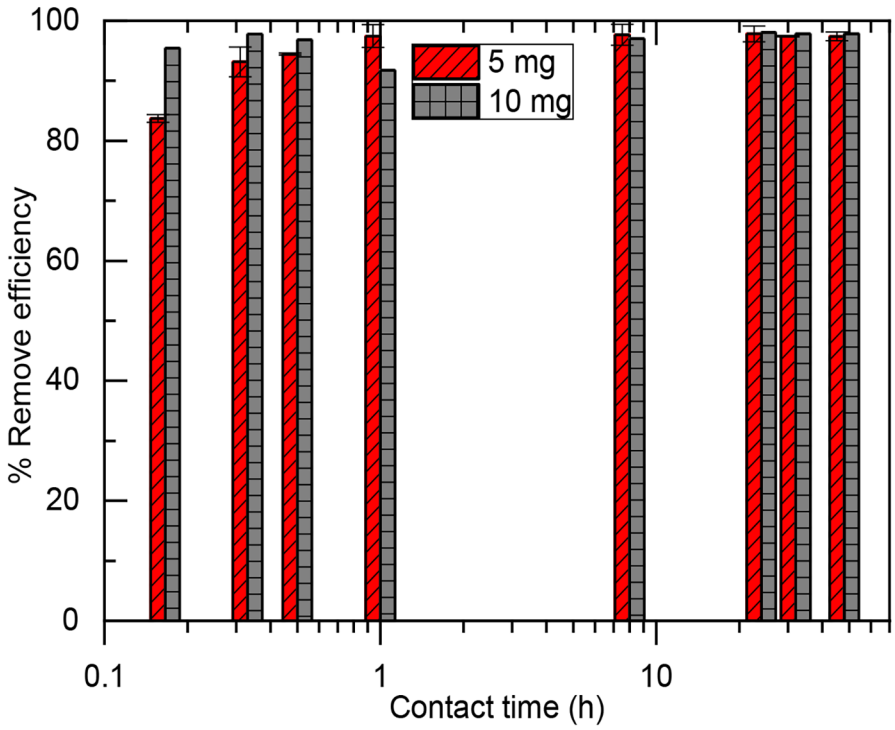

Fig. 6 ffect of contact time and adsorbent dosage (5 and 10 mg, corresponding to 5000 μg L^{-1} and 10,000 μg L^{-1}) on the arsenic removal

where $k_1(h^{-1})$ is the pseudo-first-order adsorption rate constant, k_2 (mg g^{-1} h^{-1}) is the pseudo-second-order rate constant of the kinetic model, q_e(mg g^{-1}) and q_t(mg g^{-1}) are the amounts of As adsorbed at equilibrium and at any contact time, t (h). The results obtained for each of the kinetic models showed a correlation coefficient constant (R^2) (that significantly describes the models) of 0.88 and 0.99 for the pseudo-first order and pseudo-second order models,

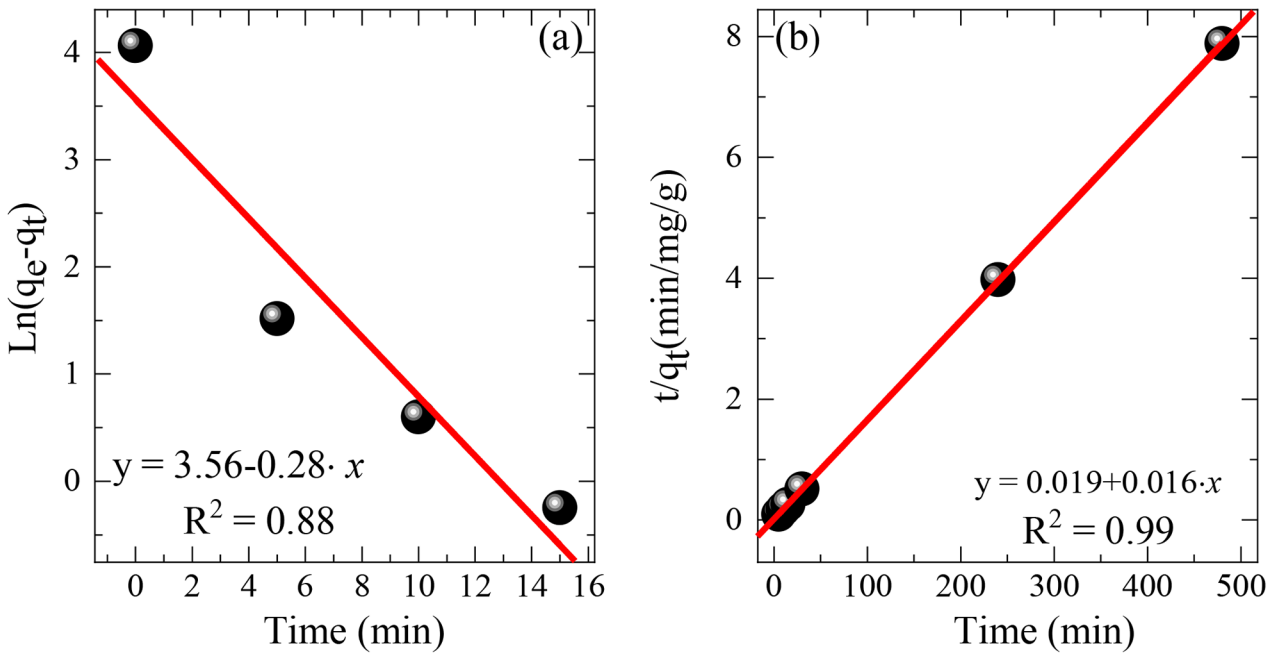

Fig. 7 dsorption kinetics for pseudo-first-order and pseudo-second-order models applied for arsenic adsorption onto magnetite nanoparticles

respectively. The significant value of R^2 indicates that the adsorption kinetics follows the pseudo-second-order model that showed a better fit for As (V). This model suggests that the mechanism of adsorption is chemical interaction or chemisorptions [45]involving valence forces through sharing or exchange of electrons between As and Fe_3O_4 NPs [24]. Both models give the calculated value of q_e, along with the prediction of q_t. According to the fitting results, the value of q_e for the pseudo-first-order model and the pseudo-second-order model were found to be 35.2 mg g^{-1} and 60.97 mg g^{-1}, respectively. Then, the q_e value obtained from the pseudo-second-order model is very close to the experimental value, q_{e-exp}≈58.2 mg g^{-1} confirming the excellent agreement with the model, whereas, for pseudo-first-order model, the q_e is much lower than q_{e-exp}. This fact also indicates that the pseudo-second-order model better describes the experimental data to explain the arsenic adsorption carried out by Fe_3O_4 NPs. Hence, the adsorption process is controlled by a chemisorption rate occurred during the arsenic removal process.

Adsorption isotherm models are fundamental for describing the equilibrium between the adsorbate and adsorbent, and it is also essential to investigate mechanisms of adsorption [10]. The experimental isotherm for a contact time of 8 h was analyzed from three models, the Langmuir, Freundlich, and Sips models. The results of the fits are shown in Fig. 8. The Langmuir model is based on the monolayer adsorption on the homogenous surface, and no significant interaction among adsorbed species [15], while the Freundlich model is based on the multilayer adsorption on heterogeneous surfaces sites, suggesting the multilayer adsorption of arsenic was heterogeneous (on the heterogeneous surface) [11]and it has different absorption force. The experimental adsorption data were analyzed by the Langmuir (Eq. (3)), Freundlich (Eq. (4)), and Sips (Eq. (5)) isotherm models in their lineal form given by [47–50]

$$\frac{C_e}{q_e} = \frac{1}{K_L q_{max}} + \frac{C_e}{q_{max}} \tag{3}$$

$$\log q_e = \log K_F + \frac{1}{n}\log C_e \tag{4}$$

$$\ln\left(\frac{q_e}{qmax - qe}\right) = \frac{1}{n} \cdot \ln C_e + \ln K_s \tag{5}$$

where C_e (mg L^{-1}) is the equilibrium arsenic concentration, q_e is the amount of As adsorbed, K_L (L mg^{-1}) is the Langmuir adsorption constant related to the affinity between the solute and adsorbent, and q_{max} (mg g^{-1}) is the theoretical maximum adsorption capacity. K_F (L mg^{-1}) is the Freundlich constant, and n is an empirical parameter of the maximum adsorption capacity.

The fit of the data provided R^2 value comparable with the Langmuir model (R^2≈0.993), the Freundlich model (R^2≈0.996), and the Sips model (R^2≈0.999). All of the equilibrium adsorption constants are listed in Table 1, where the values collected from the literature are included

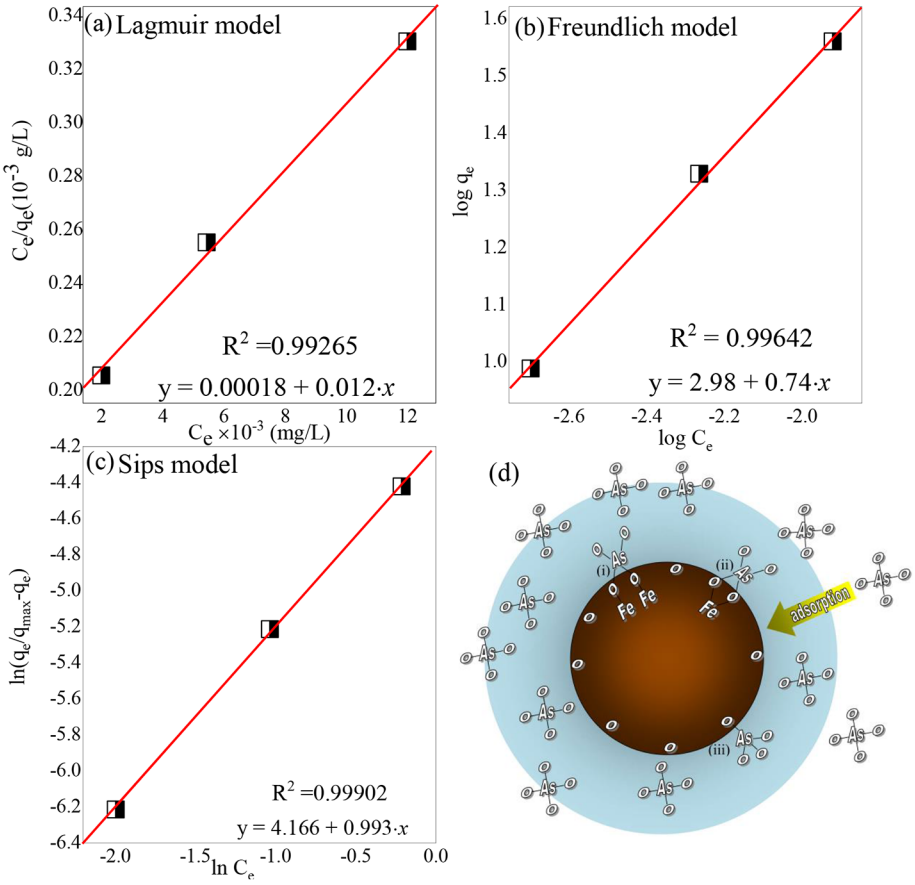

Fig. 8 Equilibrium adsorption isotherms for arsenic on magnetite. (a) Langmuir fit, (b) Freundlich fit, and (c) Sips fits for arsenic adsorption by magnetite nanoparticles. (d) schematic representation of the arsenic complexes which can be adsorbed on the surface of the particles

Table 1 Parameters assesses from the Langmuir, Freundlich, and Sips fitting models for arsenic (V) adsorption for our data (OD). * Data obtained from Ref [10] for nanoparticles of magnetite nFe_3O_4 (~ 12 nm) and commercial cFe_3O_4. ** Obtained from Ref [12] for γ-Fe_2O3 (~ 23.5 nm)

Sample	Langmuir				Freundlich			Sips		
	K_L (L/mg)	q_{max} (mg/g)	R_L	R^2	n	K_F (L/mg)	R^2	n	K_s (L/mg)	R^2
OD	67.16	81.04	0.095	0.993	1.36	964.87	0.996	1.007	64.46	0.999
nFe3O4*	0.297	66.53	0.048	0.999	1.24	4.37	0.877	-	-	-
cFe_3O_4*	0.200	39.26	0.113	0.887	1.56	2.77	0.896	-	-	-
γ-Fe_2O3**	6.025	12.74	-	0.898	10	10.50	0.724	-	-	-

for comparison. According to the results of the Langmuir fit, the values of q_{max} and K_L were found to be 81.04 mg g^{-1} and 67.16 L mg^{-1}, respectively, which suggested the formation of an adsorbed monolayer on the surface during the absorption process [16].

To determine if the adsorption process is favorable, an equilibrium parameter was defined to measure the adsorption efficiency R_L with the following expression: $R_L = 1/(1+K_LC_O)$, where C_O (mg L^{-1}) is the concentration of initial metal ions. An R_L value of 0.095 was obtained, which confirms that the adsorption process is favorable ($0<R_L<1$) by the isothermal model of Langmuir [10, 34, 37]. This is also consistent with the Freundlich constant $1/n=0.74$ which oscillates in the range of $0<1/n<1$, so the adsorption process through the Freundlich model is also considered favorable 17, 37, 51. If $n<1$, it would indicate that the adsorption of As on the surface is not favorable [11]. Thus, it was suggested that the Langmuir and Freundlich adsorption isotherm data form homogeneous and heterogeneous surfaces that are covered by adsorbed arsenic ions 10, 15, 37. To corroborate the latter, the Sips model is tested, which merged the Langmuir and the Freundlich isotherms into a single equation [49], As observed, a better correlation with the experimental data is obtained. Figure 8 (d) is present a schematic representation showing how the arsenic (V) complexes can be adsorbed on the surface of the particles. Reports about the study using the X-ray Absorption Fine Structure (EXAFS) technique 52, 54 suggested the bidentate binuclear inner-sphere complexes (i) are the most thermodynamically favored and thus the most abundant

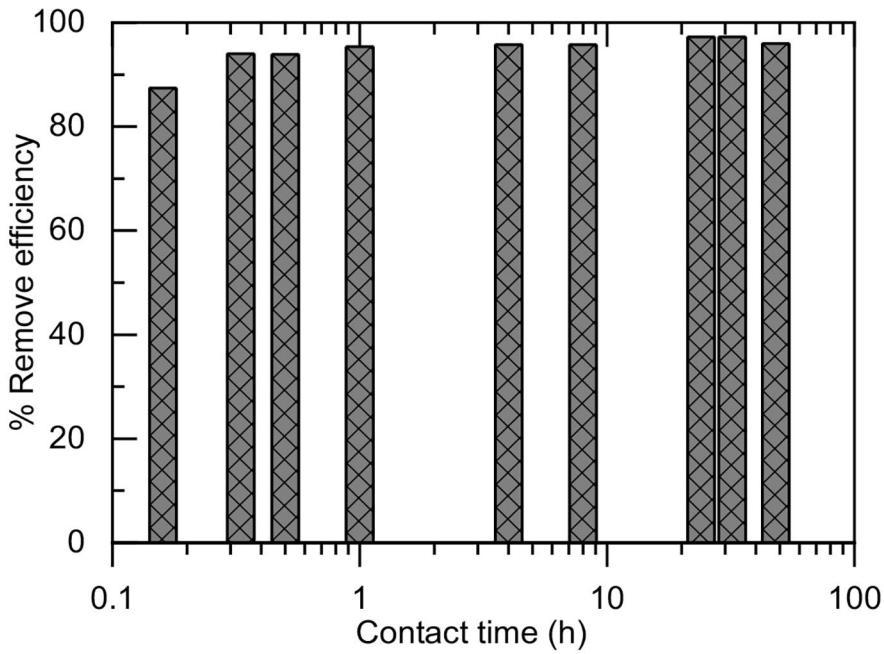

Fig. 9 The arsenic removal efficiency of Fe_3O_4 NPs as a function of the contact time for the arsenic adsorption from the Tambo river's natural water

species found on the iron oxide surface. However, the presence of the bidentate mononuclear (ii) and monodentate complexes (iii) are not likely present [53]. The magnetite NPs were evaluated for the arsenic removal from natural water samples (see Fig. 9) taken from the Tambo river in Arequipa, Peru. The arsenic content was analyzed before and after adsorption via the ICP-OES technique. Results indicated that the removal process was optimal, achieving 97.24% of total arsenic present in the water of the Tambo River. After 24 h of contact, using 5000 µg of NPs in 1 L of the river water, the initial arsenic concentration of 267 µg L^{-1} was reduced to 7.38 µg L^{-1}, which is below the WHO limit value (10 µgL^{-1}) accepted for water. Hence, one of the main advantages of using this type of adsorbent is the short contact time to get a high removal efficiency.

Conclusion

Magnetite NPs with a size of ~13 nm were successfully synthesized by the coprecipitation method. Magnetic measurements reveal the magnetic thermal relaxation of strongly interacting particles with a blocking temperature above 340 K. FTIR spectroscopy data analysis indicates that the hydroxyl groups related bands show a drastic weakening after the adsorption of As (V) likely at the particles' surface. The optimal pH value for the arsenic removal from water using Fe_3O_4 NPs is found to be 2.5, the best contact time of 60 min, and the highest efficiency of ~97% is obtained for 5000 µg $L^{-1}$of adsorbent. It is found that the adsorption kinetics is better described by the pseudo-second order model, suggesting that the adsorption process is taken by a chemisorption process with an equilibrium capacity of 60.97 mg g^{-1}. Data analysis using Langmuir's isotherm model provides a q_{max} ~ 81.04 mg g^{-1} and an RL of 0.095, and Freundlich's isothermal model provides a value of 1/n ~ 0.73, indicating that the arsenic adsorption can happen on the surface of Fe_3O_4 NPs. Meanwhile, the Sips model provides better data correlation, suggesting that the arsenic is adsorbed forming a monolayer on the NPs surface, and after the complete covering, additional layers are adsorbed. Tests of arsenic removal from a water sample collected from the Tambo river (a Peruvian river) indicate an efficiency of ~97% within 24 h, which corresponds to an arsenic reduction from 267 µg L^{-1} to 7.38 µg L^{-1}, which is below the limit established by WHO (10 µg L^{-1}). The obtained results strongly suggest that the Fe_3O_4 NPs synthesized for this work show good potential for arsenic removal from contaminated water. Although this method seems may be suitable for the arsenic removal from static water, it is important to determine the chemical stability of the magnetite NPs and their consequences on the arsenic remotion efficiency.

Acknowledgements The authors thank the financial support of the Universidad Nacional de San Agustin de Arequipa with the thesis project (Contract number: TP-061-2018 UNSA).

Declarations

Conflict of interest The authors declare no conflict of interest.

References

1. Fan Y, Jiang Y, Hu P, Chang R, Yao S, Wang B, et al. Modification of association between prior lung disease and lung cancer by inhaled arsenic: A prospective occupational-based cohort study in Yunnan, China. J Expo Sci Environ Epidemiol. 2016 Sep 13;26(5):464–70; https://doi.org/10.1038/jes.2016.22.
2. Yoshida T, Yamauchi H, Fan Sun G. Chronic health effects in people exposed to arsenic via the drinking water: Dose-response relationships in review. Toxicol Appl Pharmacol. 2004;198(3):243–52.
3. Frost FJ, Muller T, Petersen HV, Thomson B, Tollestrup K. Identifying US populations for the study of health effects related to drinking water arsenic. J Expo Anal Environ Epidemiol. 2003;13(3):231–9.
4. Gera R, Singh V, Mitra S, Sharma AK, Singh A, Dasgupta A, et al. Arsenic exposure impels CD4 commitment in thymus and suppress T cell cytokine secretion by increasing regulatory T cells. Sci Rep. 2017;7(1):1–13. https://doi.org/10.1038/s41598-017-07271-z.
5. Herschy RW. Water quality for drinking: WHO guidelines. 2012. http://www.who.int. Accessed 2012.
6. Chowdhury SR, Yanful EK. Arsenic removal from aqueous solutions by adsorption on magnetite nanoparticles. Water Environ J. 2011;25(3):429–37.
7. Yazdani F, Seddigh M. Magnetite nanoparticles synthesized by co-precipitation method: The effects of various iron anions on specifications. Mater Chem Phys. 2016;184:318–23. https://doi.org/10.1016/j.matchemphys.2016.09.058.
8. Bazrafshan E, Faridi H, Mostafapour FK, Mahvi AH. Removal of arsenic from aqueous environments using moringa peregrina seed extract as a natural coagulant. Asian J Chem. 2013;25(7):3557–61.
9. Son HX, Hao PV, Vinh HV, Hai NT, Ngan NTK, Minh DN, et al. Removal of arsenic from water using crumpled graphite oxide. Green Process Synth. 2018;7(5):404–8. https://doi.org/10.1515/gps-2018-0018.
10. Iconaru SL, Guégan R, Popa CL, Heino MM, Ciobanu CS, Predoi D. Magnetite. (Fe3O4) nanoparticles as adsorbents for As and Cu removal. Appl Clay Sci. 2016;134:128–35.
11. Nikić J, Tubić A, Watson M, Maletić S, Šolić M, Majkić T, et al. Arsenic removal from water by green synthesized magnetic nanoparticles. Water (Switzerland). 2019;11(12).
12. Zeng H, Zhai L, Qiao T, Yu Y, Zhang J, Li D. Efficient removal of As(V) from aqueous media by magnetic nanoparticles prepared with Iron-containing water treatment residuals. Sci Rep. 2020;10,9335:1–12. https://doi.org/10.1038/s41598-020-65840-1.
13. Zeng H, Yin C, Qiao T, Yu Y, Zhang J, Li D. As(V) Removal from Water Using a Novel Magnetic Particle Adsorbent Prepared with Iron-Containing Water Treatment Residuals. ACS Sustain Chem Eng. 2018;6(11):14734–42.
14. Fadli A, Komalasari, Adnan A, Iwantono, Rahimah, Addabsi AS. Synthesis of Magnetite Nanoparticles via Co-precipitation Method. IOP Conf Ser Mater Sci Eng. 2019;622(1).
15. Joshi S, Sharma M, Kumari A, Shrestha S, Shrestha B. Arsenic removal fromwater by adsorption onto iron oxide/nano-porous carbon magnetic composite. Appl Sci. 2019;9:18.
16. Monárrez-Cordero BE, Amézaga-Madrid P, Leyva-Porras CC, Pizá-Ruiz P, Miki-Yoshida M. Study of the adsorption of arsenic (III and V) by magnetite nanoparticles synthetized via AACVD. Mater Res. 2016;19:103–12.
17. Kango S, Kumar R. Magnetite nanoparticles coated sand for arsenic removal from drinking water. Environ Earth Sci. 2016;75(5):1–12.
18. Shahid MK, Phearom S, Choi YG. Synthesis of magnetite from raw mill scale and its application for arsenate adsorption from contaminated water. Chemosphere. 2018;203:90–5. https://doi.org/10.1016/j.chemosphere.2018.03.150.
19. Taleb K, Markovski J, Veličković Z, Rusmirović J, Rančić M, Pavlović V, et al. Arsenic removal by magnetite-loaded amino modified nano/microcellulose adsorbents: Effect of functionalization and media size. Arab J Chem. 2019;12(8):4675–93.
20. Mayo JT, Yavuz C, Yean S, Cong L, Shipley H, Yu W, et al. The effect of nanocrystalline magnetite size on arsenic removal. Sci Technol Adv Mater. 2007;8(1–2):71–5.
21. Yean S, Cong L, Yavuz CT, Mayo JT, Yu WW, Kan AT, et al. Effect of magnetite particle size on adsorption and desorption of arsenite and arsenate. J Mater Res. 2005;20(12):3255–64.
22. Goldberg S, Johnston CT. Mechanisms of arsenic adsorption on amorphous oxides evaluated using macroscopic measurements, vibrational spectroscopy, and surface complexation modeling. J Colloid Interface Sci. 2001;234(1):204–16.
23. Cornell RM. Schwertmann. U. The iron oxides: Structure, properties, reactions, occurrence and uses. Corros Sci. 1997;39(8):1499–500.
24. Yang JC, Yin XB. CoFe2 O4 @MIL-100(Fe) hybrid magnetic nanoparticles exhibit fast and selective adsorption of arsenic with high adsorption capacity. Sci Rep. 2017;7(June 2016):1–15; https://doi.org/10.1038/srep40955.
25. Urian YA, Medrano JJ, Quispe LT, Feliz LL, Coaquira JA. Study of the surface properties and particle-particle interactions in oleic acid-coated Fe3O4 nanoparticles. Appl Clay Sci. 2021;525,167686, https://doi.org/10.1016/j.jmmm.2020.167686.
26. García FJA, Cano DAI, Cervantes GA, Salazar SJ. Magnetic domain interactions of Fe3O4 nanoparticles embedded in a SiO2 matrix. Sci Rep. 2018;8(1):2–11.
27. Gotić M, Musić S, Mössbauer. FT-IR and FE SEM investigation of iron oxides precipitated from FeSO4 solutions. J Mol Struct. 2007;834–836(SPEC. ISS.):445–53.
28. Prasad PSR, Shiva Prasad K, Krishna Chaitanya V, Babu EVSSK, Sreedhar B, Ramana Murthy S. In situ FTIR study on the dehydration of natural goethite. J Asian Earth Sci. 2006;27(4):503–11.
29. Ruan HD, Frost RL, Kloprogge JT. The behavior of hydroxyl units of synthetic goethite and its dehydroxylated product hematite. Spectrochim Acta - Part A Mol Biomol Spectrosc. 2001;57(13):2575–86.
30. Salem Attia TM, Hu XL, Yin DQ. Synthesised magnetic nanoparticles coated zeolite (MNCZ) for the removal of arsenic (As) from aqueous solution. J Exp Nanosci. 2014;9(6):551–60.
31. Rajendran K, Balakrishnan GS, Kalirajan J. Synthesis of magnetite nanoparticles for arsenic removal from ground water pond. Int J PharmTech Res. 2015;8(4):670–7.
32. Yusoff AHM, Salimi MN, Jamlos MF. Synthesis and characterization of biocompatible Fe3O4 nanoparticles at different pH. Adv Mater Eng Technol V. 2017;1835:1–5.
33. Oke IA, Olarinoye NO, Adewusi SRA. Adsorption kinetics for arsenic removal from aqueous solutions by untreated powdered eggshell. Adsorption. 2008;14(1):73–83.
34. Chowdhury SR. Application of mixed iron oxides in subsurface remediation. 2013. https://ir.lib.uwo.ca/etd/1301.Accessed 5 Juno 2013.
35. Yao S, Liu Z, Shi Z. Arsenic removal from aqueous solutions by adsorption onto iron oxide/activated carbon magnetic composite. J Environ Heal Sci Eng. 2014;12(1):6–13.
36. Mamindy-Pajany Y, Hurel C, Géret F, Galgani F, Battaglia-Brunet F, Marmier N, et al. Arsenic in marine sediments from French Mediterranean ports: Geochemical partitioning, bioavailability and ecotoxicology. Chemosphere. 2013;90(11):2730–6. https://doi.org/10.1016/j.chemosphere.2012.11.056.

37. Fato FP, Li DW, Zhao LJ, Qiu K, Long YT. Simultaneous Removal of Multiple Heavy Metal Ions from River Water Using Ultrafine Mesoporous Magnetite Nanoparticles. ACS Omega. 2019;4(4):7543–9.
38. Manna BR, Dey S, Debnath S, Ghosh UC. Removal of arsenic from groundwater using crystalline hydrous ferric oxide (CHFO). Water Qual Res J Canada. 2003;38(1):193–210.
39. Chiban M, Carja G, Lehutu G, Sinan F. Equilibrium and thermodynamic studies for the removal of As(V) ions from aqueous solution using dried plants as adsorbents. Arab J Chem. 2016;9:988–99. https://doi.org/10.1016/j.arabjc.2011.10.002.
40. Gallegos-Garcia M, Ramírez-Muñiz K, Song S. Arsenic removal from water by adsorption using iron oxide minerals as adsorbents: A review. Min Process Extr Met Rev. 2012;33(5):301–15.
41. Alguacil, F. J. The removal of toxic metals from liquid effluents by ion exchange resins. Part XV: Iron(II)/H+/Lewatit TP208. Rev. Metal. 57, 4–9 (2021).
42. Radfard M, Yunesian M, Nabizadeh R, Biglari H, Nazmara S, Hadi M, et al. Drinking water quality and arsenic health risk assessment in Sistan and Baluchestan, Southeastern Province, Iran. Hum Ecol Risk Assess. 2019;25(4):949–65. https://doi.org/10.1080/10807039.2018.1458210.
43. Moztahida M, Jang J, Nawaz M, Lim SR, Lee DS. Effect of rGO loading on Fe 3 O 4: A visible light assisted catalyst material for carbamazepine degradation. Sci Total Environ. 2019;667(7):741–50.
44. Zhang G, Liu H, Liu R, Qu J. Adsorption behavior and mechanism of arsenate at Fe-Mn binary oxide/water interface. J Hazard Mater. 2009;168(2–3):820–5.
45. Ho YS, Mckay G. a C Om Parison of C Hem Isorptio N Kinetic M Odels Applied To Pollutant Rem Oval on Various So Rbents. 1998;76.
46. Ho YS, Ofomaja AE. Pseudo-second-order model for lead ion sorption from aqueous solutions onto palm kernel fiber. J Hazard Mater. 2006;129(1–3):137–42.
47. Sharifi S, Nabizadeh R, Akbarpour B, Azari A, Ghaffari HR, Nazmara S, et al. Modeling and optimizing parameters affecting hexavalent chromium adsorption from aqueous solutions using Ti-XAD7 nanocomposite: RSM-CCD approach, kinetic, and isotherm studies. J Environ Health Sci Engineer. 2019;17:873–88. https://doi.org/10.1007/s40201-019-00405-7.
48. Afshin S, Rashtbari Y, Vosough M, Dargahi A, Fazlzadeh M, Behzad A, et al. Application of Box–Behnken design for optimizing parameters of hexavalent chromium removal from aqueous solutions using Fe3O4 loaded on activated carbon prepared from alga: Kinetics and equilibrium study. J Water Process Eng. 2021;42(April):102113. https://doi.org/10.1016/j.jwpe.2021.102113.
49. Kua TL, Kooh MRR, Dahri MK, et al. Aquatic plant, Ipomoea aquatica, as a potential low-cost adsorbent for the effective removal of toxic methyl violet 2B dye. Appl Water Sci. 2020;10:243. https://doi.org/10.1007/s13201-020-01326-9.
50. Yousefi M, Nabizadeh R, Alimohammadi M, Mohammadi AA, Mahvi AH. Removal of phosphate from aqueous solutions using granular ferric hydroxide process optimization by response surface methodology. 2019; 158: 290–300. doi: https://doi.org/10.5004/dwt.2019.24281.
51. Rahdar S, Taghavi M, Khaksefidi R, Ahmadi S. Adsorption of arsenic (V) from aqueous solution using modified saxaul ash: isotherm and thermodynamic study. Appl Water Sci. 2019;9(4):1–9. https://doi.org/10.1007/s13201-019-0974-0.
52. Sherman DM, Randall SR. Surface complexation of arsenic(V) to iron(III) (hydr)oxides: Structural mechanism from ab initio molecular geometries and EXAFS spectroscopy. Geochim Cosmochim Acta. 2003;67(22):4223–30. https://doi.org/10.1016/S0016-7037(03)00237-0.
53. Carabante I, Grahn M, Holmgren A, Kumpiene J, Hedlund J. Adsorption of As (V) on iron oxide nanoparticle films studied by in situ ATR-FTIR spectroscopy. Colloid Surf A-Physicochem Eng Asp. 2009;346(1–3):106–13.
54. Guillaume, Morin Yuheng, Wang Georges, Ona-Nguema Farid, Juillot Guillaume, Calas Nicolas, Menguy Emmanuel, Aubry John R., Bargar Gordon E., Brown (2009) EXAFS and HRTEM Evidence for As(III)-Containing Surface Precipitates on Nanocrystalline Magnetite: Implications for As Sequestration. Langmuir 25(16) 9119-9128 10.1021/la900655v

Publisher's Note Springer Nature remains neutral with regard to jurisdictional claims in published maps and institutional affiliations.

Springer Nature or its licensor holds exclusive rights to this article under a publishing agreement with the author(s) or other rightsholder(s); author self-archiving of the accepted manuscript version of this article is solely governed by the terms of such publishing agreement and applicable law.